

FEDSM-ICNMM2010-305* +

EFFECT OF NON UNIFORM OUT-OF-PLANE ILLUMINATION AND SHEAR RATE ON THE ACCURACY OF nPIV VELOCITY MEASUREMENTS

Rana G. Khader

Dept. of Mechanical Engineering,
Texas A&M University at Qatar,
PO Box 23874, Doha, Qatar, USA
rana.khader@qatar.tamu.edu

Reza Sadr

Dept. of Mechanical Engineering,
Texas A&M University at Qatar,
PO Box 23874, Doha, Qatar, USA
reza.sadr@qatar.tamu.edu

ABSTRACT

Nano-particle image velocimetry (nPIV) uses evanescent-wave illumination to measure two velocity components, U and V , tangent to the wall in a region with thickness of order of hundred nano meters. In this region the illumination intensity decays exponentially with distance normal to the wall, z , and hence tracers closer to the wall have "brighter" and "bigger" images than those that are further away, i.e. at larger z . Moreover fluid velocity varies in this region with z and hence tracers at different distance from the wall move at different speeds. Furthermore, Brownian displacement of particle tracers in this region is comparable to the displacement due to the fluid convection. The variation in the displacement of particle images in this region, with different brightness and velocities, can bias the near-wall velocities obtained using standard correlation based PIV method.

Artificial nPIV images of nano particle in a flow field with linear out of plane velocity profile were used in this work to investigate the impact of these issues upon the accuracy of nPIV data. Uniform and Gaussian random distribution noise were added to the images to simulate electronic noise and shot noise, respectively. The artificial images were obtained and processed for various experimental parameters to incorporate different illumination profile and shear rates. The results demonstrate that non-uniform illumination affects the bias in the estimated tracer velocity for the shear flow. Non-uniform intensity also affects the bias due to Brownian diffusion; however, correction for Brownian diffusion can reduce this bias error.

1 INTRODUCTION

Over the past 15 years, there has been a lot of work on the application of micro fluidic systems in science and engineering, e.g. medical and electronics. The design of these systems often requires a better understanding of the fluid flow characteristics at sub micron scale. For most part, μ PIV [1] remains the most popular technique for measuring fluid velocity profile in micro channels.

In μ PIV fluid velocity is obtained by measuring velocity of naturally buoyant fluorescent tracers (100-500 nm diameters) added to the flow. Here the entire flow field in the micro channel is illuminated by a laser beam and the out of plane resolution is then limited by the depth of focus of the optical lens used in imaging the tracers, $O(1\mu\text{m})$ [2]. The finest near wall velocity measurements using μ PIV was recorded at a normal distance of $\sim 450\text{nm}$ [3,4]. This however is insufficient in study of velocity field at the fluid-surface interface.

Nano-particle image velocimetry (nPIV) offers the ability for near wall velocity measurement [5,6] using evanescent-wave (vs. volumetric) illumination generated by total internal reflection (TIR) at the interface between the wall and the fluid. Particle tracers located in this region are illuminated with an intensity that is exponentially decaying with distance from the wall. The characteristic length of this exponential decay is called penetration depth which is usually in the order of $O(10^{-8}\text{m})$. Out-of-focus background noise in nPIV is minimized as the depth of focus of the imaging system is usually larger than the penetration depth of the evanescent wave [7]. This method has been extended further for multilayer velocity measurement in out of plane direction (MnPIV) [8,9].

As the spatial resolution of the measurement and size of the particle tracers are reduced the displacements due to Brownian diffusion become increasingly important [7]. The wall proximity effects on the Brownian motion (or hindered Brownian motion) were verified experimentally using evanescent wave microscopy by Banerjee and Kihm [10]. Near wall Brownian motion introduces an error in the velocity measurement that cannot be averaged out [7,11]. Sadr *et al.* [12] analytically estimated the bias in velocity measurement due to hindered Brownian motion at the wall by looking at particle mismatch due to "drop out" and "drop in" of tracer particles in the illuminated region.

In addition to hindered Brownian motion, electrostatic, hydrodynamic lift due to shear and van der Waals forces affect near wall tracer movement. Huang *et al.* [13] used Monte Carlo simulation to study the effects of these forces on the displacement of tracer particles moving in the near wall region in a given time interval. Their results show that the correction factor suggested by Sadr *et al.* [12] is accurate only for moderate and long time intervals, or bigger illumination thicknesses. At smaller time intervals, or distances closer to the wall, the shear-related mobility, van der Waals forces, and surface charges play an important role that affect near wall velocity estimation using displacement of particle tracers in this region.

Both μ PIV and nPIV use common cross-correlation methods to obtain particle tracer displacement in a known time interval to obtain tracer velocity in the fluid. The image characteristics in general, and image characteristics of the particle tracers in specific, have shown to affect the obtained velocity. These include the effect of interrogation size and diameter of particle image [14], particle number in the interrogation region [15], non-uniform velocity distribution [16], noise in general, out of focus particles in the image (for μ PIV) [2], and Brownian motion effects [7,11]. The effects of non-uniform light intensity and near wall Brownian motion can affect nPIV velocity measurement especially when it is associated with fluid velocity gradient in the out of plane direction.

The aim of this paper is to study the effects of Brownian motion, light penetration profiles, and near wall velocity gradient on near wall PIV measurement. Artificially generated images are used to simulate nPIV images in the near wall region of Poiseuille flow in a microchannel. A basic description of the particle tracer movement and its illumination is outlined in Section 2. Section 3 describes the Monte Carlo simulations used to generate artificial nPIV images for particle tracers convected by a known velocity profile and Brownian diffusion coefficient. Section 4 presents the results from processing these artificial images using standard cross-correlation PIV techniques and discusses the obtained errors when compared with the actual displacements for a range of experimental parameters such as shear rate, time intervals, and light penetration profile.

2 THEORY

2.1 Evanescent Wave Particle Illumination

nPIV uses TIR to illuminate tracer particles in the near wall region at the fluid-wall interface. In this section, a brief introduction on TIR and evanescent wave characteristics will be discussed, for more details refer to [6,7].

When a light beam travelling through a transparent medium of refractive index, n_1 (e.g. glass) enters a medium of less

refractive index, n_2 (e.g. water) at an angle exceeding the critical angle, $\theta_c = \sin^{-1}\left(\frac{n_2}{n_1}\right)$, measured from the normal towards the interface, the light beam experiences TIR and is reflected back into the primary medium [17]. Some of the energy from the light beam penetrates in the secondary medium and produces a thin layer of illumination (typically a few hundred nanometers for visible light [18]) parallel to the interface wall. The intensity of this light decays exponentially with distance normal to the wall, z , as:

$$I(z) = I_0 \exp\left(-\frac{z}{z_p}\right) \quad (1)$$

where I_0 is the maximum intensity at the wall and z_p is the penetration depth:

$$z_p = \frac{\lambda_0}{4\pi n_1} \left[\sin^2 \theta - \left(\frac{n_2}{n_1}\right)^2 \right]^{-\frac{1}{2}} \quad (2)$$

λ_0 is the wavelength of the light and θ is the incident angle. Figure 1 shows a schematic of illumination arrangement used in nPIV measurement. In this case TIRF microscopy is used to image fluorescent spherical particles of radius, a , in the fluid medium from below when moving near the surface. In such cases the penetration depth is smaller than the depth of focus of the imaging system which puts all of the tracer particles in focus, eliminating any noise that might occur from out-of-focus particles. The visible region, z_v , defines the depth in which the particles can be seen, and z_c is the averaged center location of the particles visible in that region defined as $z_c = (z_v/2 + a)$.

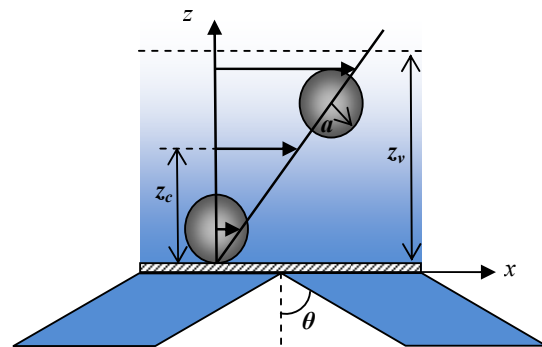


Fig. 1 Light illumination schematic in an nPIV set up

The incident energy from the evanescent wave is absorbed by the fluorescent particles, exciting the fluorophores, which then in return emit, usually, a longer-wavelength light that is picked up by the imaging system. The brightness of the particle then depends on its distance from the surface and the net power

emitted from each particle. The power collected by the imaging system can be expressed as:

$$I_p = A \exp\left(-\frac{h}{z_p}\right) \quad (3)$$

where $h=z-a$ and is the minimum distance of the tracer particle to the surface, while A is a constant that can be found in [7].

2.2 Hindered Brownian Motion

Brownian motion is the random motion of submicron particles immersed in the fluid as the result of the thermal energy of the fluid. As the length scale reduces to the submicron range, Brownian effects become an important factor in particle displacement [17].

For particles in unconfined flow the Brownian diffusion coefficient follows the Stokes-Einstein equation [19]:

$$D_\infty = \frac{kT}{6\pi\mu a}, \quad (4)$$

where k is the Boltzmann constant, and T and μ are temperature and viscosity of the fluid, respectively. In the near wall region Brownian motion is ‘‘affected’’ as a result of the additional hydrodynamic drag which exists at the wall [7]. For particles near a solid surface, the diffusion coefficient is in the tensor form that can be expressed as:

$$D = D_\infty \begin{bmatrix} \beta_\perp & 0 & 0 \\ 0 & \beta_\parallel & 0 \\ 0 & 0 & \beta_\perp \end{bmatrix} \quad (5)$$

β_\perp and β_\parallel are perpendicular and parallel correction factors, respectively, and can be approximated by the equations [20, 21]:

$$\beta_\perp = \frac{(6h^2 + 2ah)}{(6h^2 + 9ah + 2a^2)} \quad (6)$$

$$\beta_\parallel = 1 - \frac{9}{16}\left(\frac{a}{z}\right) + \frac{1}{8}\left(\frac{a}{z}\right)^3 - \frac{45}{256}\left(\frac{a}{z}\right)^4 - \frac{1}{16}\left(\frac{a}{z}\right)^5 \quad (7)$$

As the particle moves away from the wall, these correction factors tend to unity as the diffusion coefficient tends to the Stokes-Einstein value [7,11].

Displacements of a colloidal particle experiencing Brownian diffusion can be calculated using the standard Langevin equation of motion [22]. Langevin type equations describe the

temporal change in acceleration due to a stochastic force. The Brownian displacement vector, $\Delta\vec{x}$, of a spherical particle over the time interval Δt is calculated using the Langevin equation under the assumptions of Stokes flow and Brownian diffusion:

$$\Delta\vec{x} = \sum_{t=0}^{t=\Delta t} \{(\vec{\nabla} \cdot D)\delta t + \chi\delta\vec{r}\} \quad (8)$$

where χ is an array of normally distributed random numbers with a mean of zero and a standard deviation of one and $\delta\vec{r}$ is the root mean square displacement due to Brownian diffusion [11, 22]. The first term in the Langevin equation incorporates the effect of the distance of the tracer particle from the wall on the diffusion coefficient and the second term in the equation represent the random motion of the particles. Huang *et al.* [13] used a more complete form of Langevin equation that includes additional terms for electro and hydro static in addition to van der Waals forces.

3 SIMULATIONS WITH ARTIFICIAL IMAGES

Artificially generated image pairs are used in this work to study the effects of non-uniform illumination and velocity profile in combination with Brownian motion on the accuracy of nPIV image processing. This section describes the Monte Carlo simulation method and the characteristics of the artificial nPIV images.

Initially particle tracers are distributed uniformly in the first image, at $t=0$, in the near wall region of flow similar to actual experimental images. The particles are randomly distributed over an imaging region of (653×70) pixels in the ($x \times y$) direction and distance of $5z_p$ normal to the wall. Particle distribution is set by a uniform random number with a density to match that of experimental images [6].

Particle images are assumed circular with a Gaussian intensity distribution profile with the peak grayscale value calculated using Eq. (3). The images size corresponds to that of real experimental nPIV images for tracer particles of $a = 50$ nm in water at $T = 300$ K. In sub micron PIV imaging, scattered light from a small particle produces an Airy disk pattern due to diffraction limited imaging [15]. Figure 2 shows a comparison of the point-spread function of the Airy disk with that of a Gaussian profile. A good agreement is observed and, therefore, a Gaussian profile is used in this work for the base particle intensities profile in the generated images. Variations in particle image size are primarily due to variations in the particle displacement in the exponentially decaying intensity of the evanescent-wave illumination.

Two categories of noise, shot noise and electronic noise, were added to both images to improve the quality of the simulation. Shot noise (photon noise) is an inevitable feature of all

cameras and is therefore important to include in any image simulation.

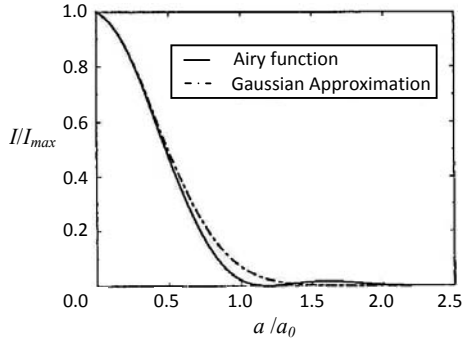


Fig. 2 Normalized intensity distribution of the Airy pattern and its approximation by a Gaussian curve [15]; a = position in the radial direction, a_0 = radius of particle image

It is a result of the instability of the number of emitted photons with a direct relationship between the square root of the local intensity at each pixel and the existing shot noise [23]. Shot noise normally follows a Poisson distribution [24] which can be approximated as Gaussian [25]. Shot noise for the images was added by finding the average intensity, I_{av} , of a real image and setting the mean and standard deviation of the Gaussian distribution as I_{av} and $\sqrt{I_{av}}$, respectively. Image gain and image filtering are then incorporated as well as uniform white noise distribution which accounts for other noise sources e.g. intensification, read-out and dark current (electronic noise). The scaling factors for the two noise models (Gaussian and random uniform distribution) were varied until the intensity profile of the simulated image matched that of the real image in Figure 3.

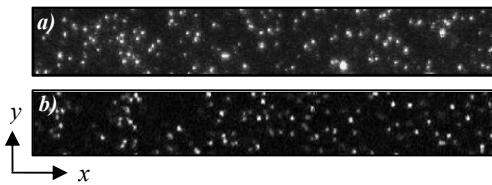


Fig. 3 A comparison between an a) real image b) simulated image

Figure 4 shows a typical intensity profile for the simulated image compared with that of experimental one extracted from Figure 3.

Tracer particles in the first image were moved to the new position in the second image via Monte Carlo simulations. Particle displacements are calculated for a PIV time interval Δt as the result of Brownian motion and fluid convection. Brownian diffusion was incorporated to displace the particles using the Langevin and Stokes-Einstein equations with the corresponding correction factors for near wall hindrance.

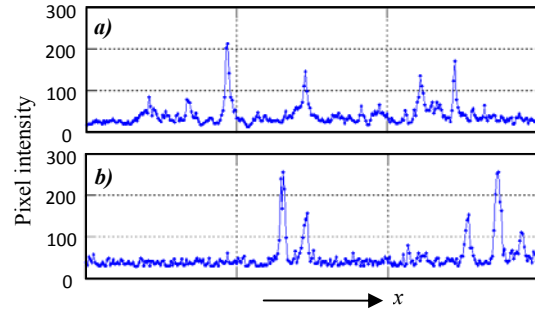


Fig. 4 A comparison of the intensity profile between a) real image b) simulated image

The time step in Monte Carlo simulation, $\delta t = 5 \mu s$, was chosen an order of magnitude larger than the Brownian diffusion time for the particle tracers. Displacements of each particle during the PIV time interval were calculated over a sequence of constant time steps, where $\Delta t = \sum \delta t$, and their final positions are used in the second image. Particle collisions at the wall were considered to be perfectly elastic satisfying the Neumann boundary condition [11].

Image pairs were produced for three different light profiles of uniform, linearly decaying, and exponential decaying intensity over the observation depth of the camera, z_v . Real flow conditions would entail shear flow, exponentially decaying light intensity, and the presence of hindered and no Brownian motion. The other hypothetical cases were also studied to compare and better understand the effects of shear, lighting, and Brownian motion on the flow measurement.

Steady shear flow velocity profile was assumed with a velocity component parallel to the wall in x direction, where $u(z) = G \cdot z$ and G is the shear rate. The range of variation for shear rate is that of a typical Poiseuille flow in microchannels [9, 22]. This range of G in the wall region was confirmed by simulating a no-slip fluid flow in a micro channel using FLUENT. The shear rate at the fluid-wall interface in a rectangular micro channel of height $150 \mu m$ and width $300 \mu m$ with a mass flow rate of $1.58 \times 10^{-6} \text{ kgs}^{-1}$ is 2000 s^{-1} .

Simulations were performed to investigate the number of image pairs needed for the convergence of the final results. Figure 5 shows the obtained velocity for a case of shear flow with exponentially decaying intensity and hindered Brownian motion normalized by the velocity at z_c . It is observed that the calculated velocity converges to a constant value as the number of the processed images increases. All the results in this work are obtained by studying up to 2500 independent image pairs each containing five interrogation zones. This will provide a statistical averaging over more than 12000 independent samples.

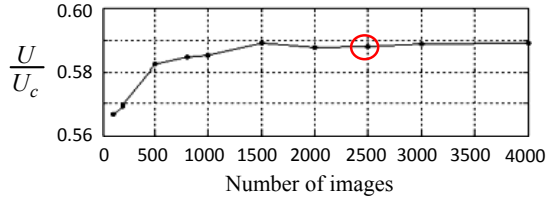


Fig. 5 Normalized velocity against number of images for shear flow, exponentially decaying light intensity and with Brownian motion; $G=2000s^{-1}$ and $\Delta t=6ms$

4 RESULTS

A standard FFT-based cross correlation program with a Gaussian pick finding algorithm was used to obtain tracer displacements in the image [8]. The image is divided into interrogation windows of size 186×68 pixels creating 5 adjacent data points for each image pair with their midpoints centered along the centerline in the y direction with an overlap of $\sim 40\%$. The search region for cross-correlation is specified by the search radius, r_s , in x and y directions and is set to 18×18 pixels. This radius was chosen based on the maximum displacement at the centre of the visible region after an average time interval for a shear rate of $G=3000s^{-1}$. This enabled us to observe the effect of the size of search radius on the velocity profiles for each case. The image processing code outputs a data file containing the displacements and standard deviations of the particles which can then be used to plot the velocity profiles and the errors associated with the test. This will provide a total number of up to 12000 statistically independent samples to be used to obtain mean velocities and standard deviations of the calculated displacements.

Figure 6 shows the results of the image cross-correlation image processing for a uniform flow distribution for the case of uniform light intensity compared with an exponentially decaying intensity in an evanescent field for different PIV time intervals. The time interval is normalized based on the center line velocity, U_c , and search window radius, $\Omega = \frac{\Delta t \cdot U_c}{r_s}$. As expected these figures show that the tracer, and fluid velocity, can be faithfully obtained up to the point where the tracer particles start moving out of the interrogation window, $\Omega = 1$. Similar trends were obtained for cases of uniform flow and no Brownian motion for all light profiles as expected.

The effect of shear for a non-uniform illumination on the calculated velocity is investigated by comparing the results for different illumination profile in the measurement region. Figure 7 shows the result of PIV data reduction for different light intensity profiles of uniform, linear, and exponential for the case of zero Brownian diffusion at different shear rates. The trend in the case of uniform illumination is similar to that of Figure 6a for uniform flow field.

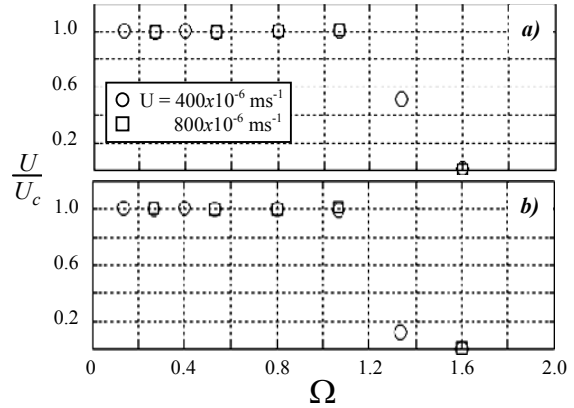


Fig. 6 Calculated velocities in a uniform flow in the presence of Brownian motion for a) uniform flow and uniform light intensity and b) uniform flow and exponential light intensity

For the case of shear flow, however, the starting point for the deviation from the actual fluid velocity at the center is at $\Omega \cong 0.75$, as the particles at the top of the measurement volume, $z = z_v$, exit the measurement domain sooner than the ones in the center, $z = z_c$, where the velocity is normalized against.

Figure 7 shows the affects of illumination profile on the estimated velocity in a shear flow field. The dimmer tracer particles that are further away from the wall move faster than the brighter tracer particles that are closer to the wall. This non uniformity biases the estimated velocity as whole towards the region lower than the velocity in the geometrical middle point in the illumination zone, i.e. U_c . By comparing the trends of linear intensity profile and exponential intensity profile it is observed that the sharper the non uniformity the more the bias on the estimated velocity.

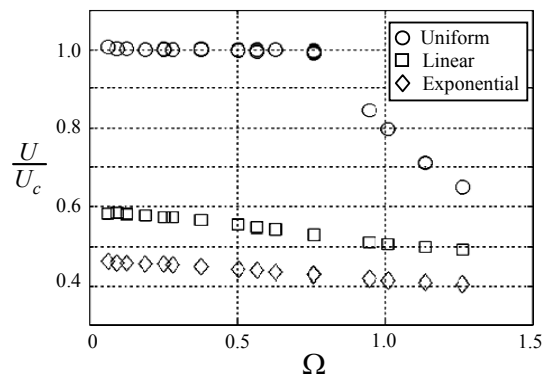


Fig. 7 Effects of lighting profile on shear flow velocity measurement. Each line contains all the shear rates study in this work, i.e. $G=1000, 1500, 2000,$ and $3000 s^{-1}$

The accuracy of the velocities obtained in this work can be characterized by statistical properties of the 12000 samples used to calculate the averaged value. Standard deviation of the velocity samples present 63% confidence level for the calculated ensemble average. Figure 8 shows the standard

deviation for the estimated average velocities, σ , for the case of uniform intensity profile in Figure 7. As the PIV time step increases the standard deviation rapidly increases to a maximum value. This is the result of the fact that tracer particles in the image are displaced at different magnitude in the image until they reach the limit of exiting the interrogation window. After that point the standard deviation remains at fairly same level and its normalized value by center line velocity shows a reduction.

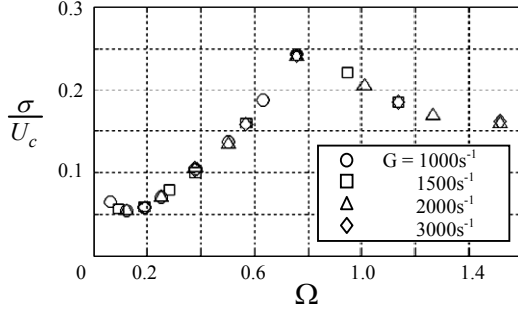


Fig. 8 Standard deviation for the estimated average velocities for shear flow with uniform intensity profile

As discussed earlier in this work Brownian motion of particles traces in the near wall region introduces bias and uncertainty in PIV velocity measurement in this region. One source of the error is due to the fact that the particles move randomly in all direction in the interrogation region and therefore introduce a noise into the calculation of the regional velocity [7]. The bias error is the result of Brownian motion in a non-uniform velocity field. Even the tracer particles that came back to the same observation region (matched particles) have visited regions with different velocities during the PIV time interval. As the result of these visits these particles are convected at a different velocity than the velocity of their position in the flow field in the time of PIV imaging.

Sadr *et al.* [12] used mathematical description of the hindered Brownian motion for the particles in combination with convective movement in the near wall velocity field of a viscous flow to derive a correction factor for the averaged displacement of particle tracers when compared to the geometrical average. The average value for the actual displacement of the particle tracers in the artificial images are used to calculate $\langle U \rangle$ using the Monte Carlo simulation. Figure 9 shows the normalized average velocity for the matched particles in the image, $\langle U \rangle / U_c$, where the average center position $U_c = z_c \cdot G$, is plotted against normalized Brownian time, $\Omega_* = \frac{D_z \Delta t}{(z_v + 0.8r)^2}$ [12]. This plot shows a good agreement with the analytically derived correction factor obtained by Sadr *et al.* [12],

$$F(\Omega_*) = 0.21 + (1 - 0.21) \exp\left\{-1.72\sqrt{\Omega_*}\right\} + 0.86\sqrt{\Omega_*} \quad (9)$$

and the results obtained by [13]. It is worth mentioning that part of the difference between the analytical correction factor and the results of this work is due to the inherent weakness in the proposed model of Sadr *et al.* in the range of Ω_* for this work [13].

The results presented in Figure 9 demonstrate the actual displacement of Brownian particle tracers in shear flow. It does not, however, account for the effects of the processing method that is cross-correlation averaging for the case of this work. Figure 10a shows average particle tracer velocity obtained from PIV processing at different PIV time interval for several shear rates studied in this work. This figure shows that the estimated velocity is underestimated for all shear values in this work when compared with the geometrical average velocity even at the smallest PIV time interval. Figure 10b shows the estimated velocity after application of the Brownian correction factor, $F(\Omega_*)$.

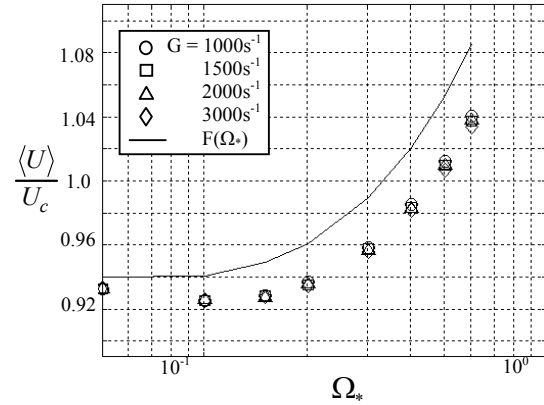


Fig. 9 Actual convected velocity of the particle tracers in a shear flow in this study compared with the suggested model by Sadr *et al.* [12]

It is observed that application of the correction factor results in unifying different trends for different shear rates and reduces the initial offset error. However, it fails to introduce a major correction in the introduced bias. This is due to the fact that the observed bias is mostly the result of out of plane non-uniform velocity field when combined with Brownian diffusion. The error can be attributed to the use of image processing (vs. theoretical calculations) which is evident in all the light illumination profiles after applying the correction factor.

Figure 11 shows the results for the cases of uniform light, linear, and exponentially decaying light illumination in shear flow with Brownian motion. Similar to the patterns observed in Figure 7, the change in the illumination profile reduces the obtained PIV velocity. Moreover Brownian motion affects the error in the calculated velocity at a different form depending on the illumination pattern.

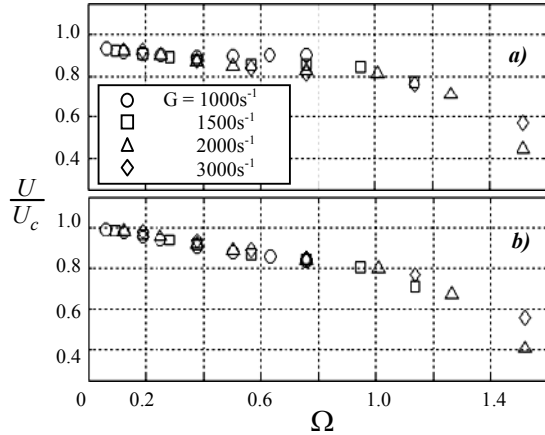


Fig. 10 Calculated nPIV velocity in shear flow with uniform illumination and Brownian motion *a)* before and *b)* after applying the Brownian correction factor

For uniform illumination the calculated velocity is underestimated when compared with the case of no Brownian motion, as observed in results of Figures 7. However, the underestimation of the calculated velocities for the non-uniform illumination is slightly reduced and dependent to the values of shear rate even at small PIV time intervals. This trend can be explained as Brownian diffusion causes particle mismatch, as well as changing their brightness and displacement by altering the z position of the particles. It can also be seen in Figure 11 that the normalized velocity initially increases with normalized time and then begins to decrease as time progresses.

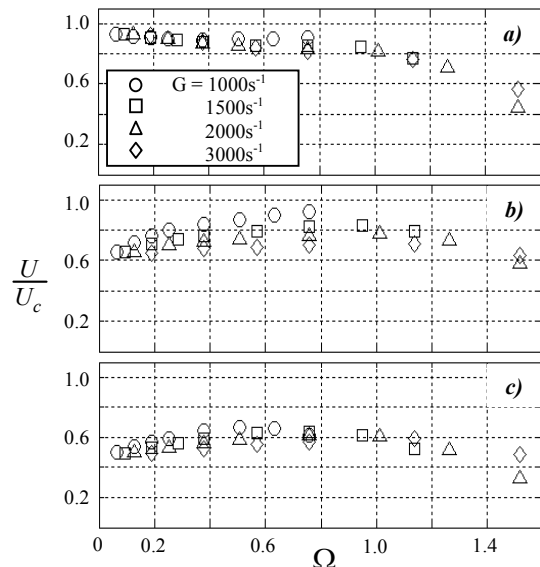


Fig. 11 Calculated nPIV velocity for Brownian particle tracers in shear flow with different illumination profile *a)* uniform light, *b)* linear light profile *c)* exponential light profile

Figure 12 shows normalized standard deviation, σ/U_c , as a function of PIV time step for different cases of light intensity profile and shear rates. It is observed that for uniform intensity

the standard deviation is nearly independent of shear rate for $\Omega < 0.7$ at a value of $\sigma/U_c \approx 0.08$. However, for the case of exponential illumination decay profile, both shear rate and PIV time interval have clear effects on the standard deviation of the results. It is also clear that for exponential illumination decay profile the normalized standard deviation is lower for the cases of higher shear rates.

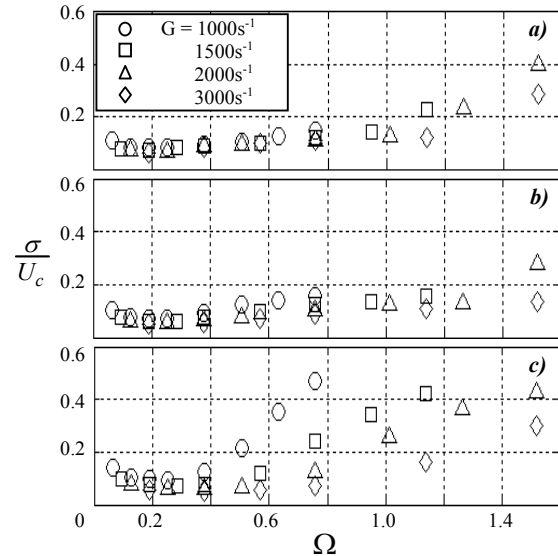


Fig. 12 Standard deviation of the calculated nPIV velocity for shear flow in *a)* uniform light, *b)* linear light and, *c)* exponential light intensity profile

Particles at the near-wall region are brighter thus have a greater contribution in cross-correlation analysis. The presence of the wall, thus hindered Brownian motion, pushes these particles away causing them to travel at higher velocities therefore overestimating the velocities.

On the other hand, the velocities of the dimmer particles further away from the wall could well be unidentified during cross-correlation causing underestimation of their velocities. It is therefore important to take into consideration the bias that arises from both the light illumination and hindered Brownian motion.

5 CONCLUSIONS

Effects of hindered Brownian motion, non uniform illumination, and out of plane velocity profiles are investigated on PIV data reduction method. For evanescent-wave illumination the illumination intensity decays exponentially with distance normal to the wall and hence tracer particles closer to the wall have "brighter" and "bigger" images than those that are further away. Moreover fluid velocity varies in this region with z and hence tracers further away from the wall move faster. These effects combined with hindered Brownian displacement of particle tracers in this region introduce error

for the near-wall velocities obtained using standard nPIV method.

The results of Monte Carlo simulation shows that the effect of light intensity variation, non-uniform out of plane velocity profile, and Brownian motion of sub micron particle tracers non linearly affect the accuracy of the estimated PIV velocities. The correction for Brownian diffusion can slightly reduce this bias error.

ACKNOWLEDGEMENTS

This work was supported by Qatar Foundation through Texas A&M at Qatar. The authors would like to thank Dr. Anoop Kanjirakat for providing assistance in obtaining CFD results.

REFERENCES

- [1] Santiago et al, 1998, A particle image velocimetry system for microfluidics, *Experiments in Fluids*, **25**, pp. 316-319.
- [2] Olsen, M. G., and Adrian, R.J., 2000, "Out-of-Focus Effects on Particle Image Visibility and Correlation in Microscopic Particle Image Velocimetry," *Experiments in Fluids*, **7**, S166-S174.
- [3] Trethewey, D. C., and Meinhart, C. D., 2002, "Apparent fluid slip at hydrophobic microchannel walls," *Physics of Fluids*, **14**, L9-L12.
- [4] Trethewey, D. C., and Meinhart, C. D., 2004, "A generating mechanism for apparent fluid slip in hydrophobic microchannels," *Physics of Fluids*, **16**, pp. 1509-1515.
- [5] Zettner, C. M., and Yoda, M., 2003, "Particle Velocity Field Measurements in a Near-Wall Flow using Evanescent Wave Illumination," *Experiments in Fluids*, **34**, pp. 115-121.
- [6] Sadr, R., Yoda, M., Zheng, Z., and Conlisk A. T., 2004, "An Experimental Study of Electro-Osmotic Flow in Rectangular Microchannels," *Journal of Fluid Mechanics*, **506**, pp. 357-367.
- [7] Sadr, R., Li, H., and Yoda, M., 2005, "Impact of Hindered Brownian Diffusion on the Accuracy of Particle-Image Velocimetry using Evanescent-Wave Illumination," *Experiments in Fluids*, **38**, pp. 90-98.
- [8] Li, H., Sadr, R., and Yoda, M., 2006, "Multilayer Nano-Particle Image Velocimetry," *Experiments in Fluids*, **41**, pp. 185-194.
- [9] Li, H., and Yoda, M., 2008, "Multilayer Nano-Particle Image Velocimetry (MnPIV) in Microscale Poiseuille Flows," *Measurement Science and Technology*, **19**, 075402.
- [10] Banerjee, A., and Kihm, K. D., 2005, "Experimental Verification of Near-Wall Hindered Diffusion for the Brownian Motion of Nanoparticles using Evanescent Wave Microscopy," *Physics Review E*, **72**, 042101/1-4.
- [11] Sadr, R., Li, H., and Yoda, M., 2005, "Bias Due to Hindered Brownian Diffusion in Near-Wall Velocimetry," 6th International Symposium on Particle Image Velocimetry, Pasadena, California, USA.
- [12] Sadr, R., Hohenegger, C., Li, H., Mucha, P. J., Yoda, M., 2007, "Diffusion-Induced Bias in Near-Wall Velocimetry," *Journal of Fluid Mechanics*, **57**, pp. 443-456.
- [13] Huang, P., Guasto, J. S., and Breuer, K., 2009, "The Effects of Hindered Mobility and Depletion of Particles in Near-Wall Shear Flows and the Implications for nanovelocimetry," *Journal of Fluid Mechanics*, **637**, pp. 241-265.
- [14] Grant, I., 1997, "Particle Image Velocimetry: A Review," *Proceedings of the Institution of the Mechanical Engineers, Part C*, **211**, pp. 55-76.
- [15] Raffel, M., Willert, C.E., and Kompenhans, J., 1998, *Particle Image Velocimetry: A Practical Guide*, Springer, Berlin, Germany.
- [16] Willert, C. E., and Gharib, M., 1991, "Digital Particle Image Velocimetry," *Experiments in Fluids*, **10**, pp. 181-193.
- [17] Azzopardi, F., and Stewart, B., 1995, *Accessible Physics for A-Level: A Guided Coursebook*, Macmillan, Hampshire, UK.
- [18] Yoda, M., and Sadr, R., 2004, "Nano-Particle Image Velocimetry (nPIV): A New Technique for Measuring Near-Wall Velocity Fields with Submicron Spatial Resolution," 42nd AIAA Aerospace Sciences Meeting, AIAA-2004-754.
- [19] Einstein, A., 1905, "Über die von der molekularkinetischen Theorie der Wärme geforderte Bewegung von in ruhenden Flüssigkeiten suspendierten Teilchen," *Ann Physics*, **17**, pp. 549.
- [20] Bevan, M. A., and Prieve, D. C., 2000, "Hindered Diffusion of Colloidal Particles Very Near to a Wall: Revisited," *Journal of Chemical Physics*, **113**, pp. 1228-1236.
- [21] Faxén, H., 1922, "Der Widerstand gegen die Bewegung einer starren Kugel in einer zähen Flüssigkeit, die zwischen zwei parallelen ebenen Wänden eingeschlossen ist," *Annals of Physics*, **68**, pp. 89-119.
- [22] Clark, A. T., Lal, M., and Watson, G. M., 1987, "Dynamics Of Colloidal Particles In The Vicinity of an

Interacting Surface,” Faraday Discussion of the Chemical Society, **83**, pp. 179-191.

[23] Dussault, D., and Hoess, P., 2004, “Noise Performance Comparison of ICCD with CCD and EMCCD Cameras,” Proceedings of SPIE, **5563**, pp. 195-204.

[24] Frenkel, A., Sartor, M. A., and Wlodawski, M. S., 1997, “Photon-Noise-Limited Operation of Intensified CCD Cameras,” Applied Optics, **36**, pp. 5288-5297.

[25] Attwood, G., Clegg, A., Dyer, G. and Dyer, J., 2009, Statistics 2: Edexcel AS and A Level Modular mathematics, A Pearson Company, UK.